Metallomics

Integrated biometal science

www.rsc.org/metallomics

Volume 4 | Number 9 | September 2012 | Pages 853–1006

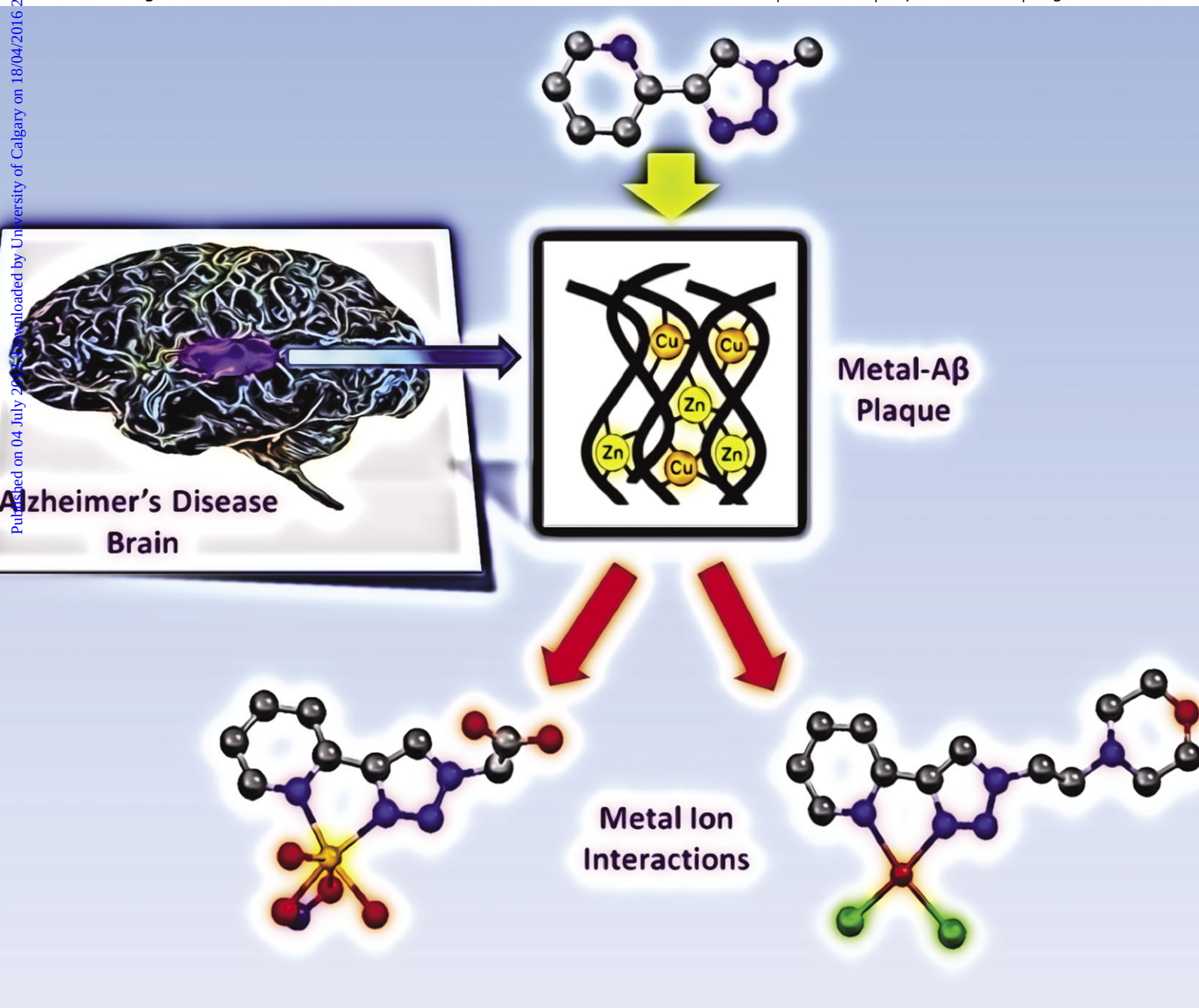

ISSN 1756-5901

RSC Publishing

PAPER

Mi Hee Lim, Tim Storr *et al.*

Dual-function triazole-pyridine derivatives as inhibitors of metal-induced amyloid-β aggregation

Indexed in MEDLINE!

Metallomics

Cite this: *Metallomics*, 2012, **4**, 910–920

www.rsc.org/metallomics

PAPER

Dual-function triazole–pyridine derivatives as inhibitors of metal-induced amyloid-β aggregation†‡

Michael R. Jones,[a] Erin L. Service,[a] John R. Thompson,[a] Michael C. P. Wang,[a] Isaac J. Kimsey,[b] Alaina S. DeToma,[b] Ayyalusamy Ramamoorthy,[bc] Mi Hee Lim*[bd] and Tim Storr*[a]

Received 14th June 2012, Accepted 4th July 2012
DOI: 10.1039/c2mt20113e

Dysregulated metal ions are hypothesized to play a role in the aggregation of the amyloid-β (Aβ) peptide, leading to Alzheimer's disease (AD) pathology. In addition to direct effects on Aβ aggregation, both Cu and Fe can catalyze the generation of reactive oxygen species (ROS), possibly contributing to significant neuronal toxicity. Therefore, disruption of metal–Aβ interactions has become a viable strategy for AD therapeutic development. Herein, we report a new series of dual-function triazole–pyridine ligands [4-(2-(4-(pyridin-2-yl)-1*H*-1,2,3-triazol-1-yl)ethyl)-morpholine (**L1**), 3-(4-(pyridin-2-yl)-1*H*-1,2,3-triazol-1-yl)propan-1-ol (**L2**), 2-(4-(pyridin-2-yl)-1*H*-1,2,3-triazol-1-yl)acetic acid (**L3**), and 5-(4-(pyridin-2-yl)-1*H*-1,2,3-triazol-1-yl)pentan-1-amine (**L4**)] that interact with the Aβ peptide and modulate its aggregation *in vitro*. Metal chelation and Aβ interaction properties of these molecules were studied by UV-vis, NMR spectroscopy and X-ray crystallography. In addition, turbidity and transmission electron microscopy (TEM) were employed to determine the anti-aggregation properties of **L1–L4**. All compounds demonstrated an ability to limit metal-induced Aβ aggregation. Overall, our studies suggest the utility of the triazole–pyridine framework in the development of chemical reagents toward inhibitors for metal-triggered Aβ aggregation.

Introduction

Neurodegenerative diseases, such as Alzheimer's disease (AD), Parkinson's disease, Creutzfeldt–Jakob disease, and amyotrophic lateral sclerosis are all defined by the gradual loss of neuronal cell populations, protein aggregation, and extensive evidence of oxidative stress.[1–4] AD is a progressive neurodegenerative disorder initially affecting brain regions involved in learning and memory, eventually resulting in death. Currently, almost six million North Americans suffer from AD, and this number is expected to increase sharply in the next 20 years.[5] The increased incidence of neurodegenerative disease, in particular AD, and the lack of effective treatment strategies make this a very important research area.[1,6,7]

Diagnosis of AD, as opposed to other forms of dementia, requires *post mortem* examination of the brain to determine the severity of neuropathological hallmarks of the disease: Aβ plaques and neurofibrillary tangles.[3] Aβ plaques are extracellular deposits mainly composed of fibrils of Aβ peptides. The Aβ peptide is a proteolytic product of the amyloid precursor protein (APP), an integral membrane glycoprotein[8] that may play a role in metal (Cu/Fe) trafficking.[9] The enzymes responsible for APP cleavage are termed the α-, β-, and γ-secretases,[10] and through a series of cleavage events afford Aβ peptides as predominantly $Aβ_{1–40}$ or $Aβ_{1–42}$ (a 40- or 42-residue peptide). The Aβ peptide has been found in three general forms in the brain: membrane-associated, aggregated, and soluble. In healthy individuals, most of the Aβ is membrane-associated, but in individuals with AD the aggregated and soluble fractions increase considerably.[11] The amyloid hypothesis has long been the dominant theory to explain the cause of AD, postulating that Aβ plaque depositions or partially aggregated soluble Aβ, trigger a neurotoxic cascade causing AD pathology.[7,12] Soluble forms of Aβ better correlate with memory impairment and AD progression;[13] however, nearly all aggregated forms exhibit toxicity. Recent studies have shown that Aβ aggregates modify the functional properties of nearby neurons,[14] and that Aβ clearance following bexarotene administration in murine models leads to behavioural improvement.[15] The recent FDA approval of the Aβ plaque imaging

[a] *Department of Chemistry, Simon Fraser University, Burnaby, BC V5A1S6, Canada. E-mail: tim_storr@sfu.ca*
[b] *Department of Chemistry, University of Michigan, Ann Arbor, Michigan, 48109, USA*
[c] *Biophysics, University of Michigan, Ann Arbor, Michigan, 48109, USA*
[d] *Life Sciences Institute, University of Michigan, Ann Arbor, Michigan, 48109, USA. E-mail: mhlim@umich.edu*
† This article is part of a themed issue on Emerging Investigators.
‡ Electronic supplementary information (ESI) available. CCDC 886726 and 886727. For ESI and crystallographic data in CIF or other electronic format see DOI: 10.1039/c2mt20113e

agent (Florbetapir) will be an important step forward for early diagnosis of AD.[16]

Evidence of oxidative stress is widespread in AD, with early neuronal and pathological changes showing indications of oxidative damage.[17] The brain is particularly susceptible to oxidative damage due to the high rate of metabolic activity coupled with relatively low antioxidant levels and low tissue regenerative capacity.[2] The cause of oxidative stress in AD has been attributed to a number of factors, including impaired cellular energy metabolism and/or Fenton-type processes involving redox-active metal ions (*e.g.*, Fe, Cu).[3,4,18–20] Under normal circumstances, metal ions are tightly regulated.[21] However, evidence implicates metal ion dysregulation in the pathology of AD.[4,20,22] Amyloid plaques have been described as 'metallic sinks' because remarkably high concentrations of Fe, Cu, and Zn have been found within these deposits in AD brains.[23,24] While extracellular levels of Cu and Zn ions increase in AD (accumulation in amyloid), intracellular ion levels decrease, exemplifying a breakdown in the homeostasis of these biologically important metal ions. *In vitro* studies have shown that the interaction of Aβ with metal ions leads to precipitation,[25] and in addition, metal–Aβ interactions initiate the formation of soluble oligomers, potentially implicating metal ions in the formation of these more mobile toxic forms of Aβ.[26] Further *in vitro* studies have demonstrated that Cu and Fe potentiate the neurotoxicity of Aβ *via* redox-cycling and the production of ROS in the presence of dioxygen.[27]

While the role of metal ions in the etiology of AD remains to be determined, targeting and controlling metal–Aβ peptide species is a viable therapeutic strategy. Metal chelators can solubilize Aβ plaque deposits[28] and, more impressively, show promise as AD therapeutics.[29,30] An early clinical study with the strong metal ion chelator desferrioxamine (DFO) showed a significant decrease in the rate of cognitive decline of treated subjects compared with the control group over a 24-month period.[29] However, the long-term use of strong metal chelators that are not tissue-specific likely affects the homeostasis of numerous biometals and the normal physiological functions of essential metal-requiring biomolecules such as metalloenzymes. Recent work with the moderate metal-binding agent clioquinol has shown the promise of chelation therapy in both animal models and human trials.[31] Advances have been made in the targeted delivery of chelating agents for AD therapy *via* activation by enzymes[32,33] and hydrogen peroxide.[34] In addition, the design of metal-binding agents that employ Aβ targeting functions also offers a mechanism to improve the activity of this class of compounds. Incorporating or linking a metal coordination site to the Aβ-binding agents, such as thioflavin-T and *p*-I-stilbene, has afforded a class of bifunctional agents that can influence metal-induced Aβ aggregation. A summary of the approaches described above is highlighted in Fig. 1.

In this work we have studied a series of 1,2,3-triazolyl-pyridine (TriPy) compounds as bifunctional reagents for targeting metal–Aβ species in AD (Fig. 2). The molecules 4-(2-(4-(pyridin-2-yl)-1*H*-1,2,3-triazol-1-yl)ethyl)morpholine (**L1**), 3-(4-(pyridin-2-yl)-1*H*-1,2,3-triazol-1-yl)propan-1-ol (**L2**), 2-(4-(pyridin-2-yl)-1*H*-1,2,3-triazol-1-yl)acetic acid (**L3**), and 5-(4-(pyridin-2-yl)-1*H*-1,2,3-triazol-1-yl)pentan-1-amine (**L4**) were synthesized in a modular fashion using Cu-catalyzed alkyne/azide

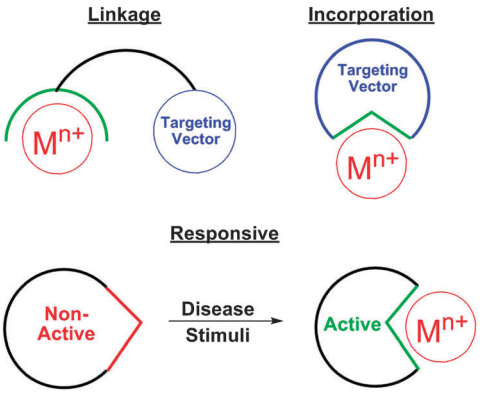

Fig. 1 Three approaches used to design molecules to disrupt the metal–Aβ interaction and reactivity. **Linkage**: A metal sequestration site is anchored to an Aβ peptide targeting vector. **Incorporation**: The Aβ peptide targeting vector includes a metal binding site. **Responsive**: A pro-drug is activated by a disease-related trigger.

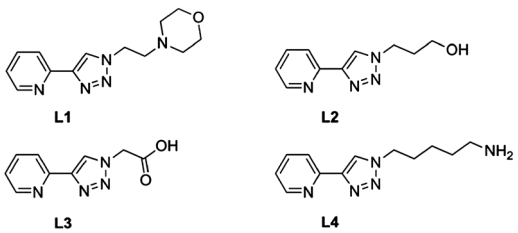

Fig. 2 Chemical structures of a series of triazole–pyridine ligands (**L1–L4**).

cycloaddition (click) chemistry.[35,36] In each case the metal binding site is identical, and formed *via* click chemistry, allowing for the correlation of biological properties with side-chain functional groups. Fe,[37] Cu,[38] and Re[39] complexes of the TriPy framework have been recently reported for C–H activation, magnetism, and radiochemistry applications. The characterization of the metal chelation and Aβ interaction properties of **L1–L4**, along with evaluation of their reactivity toward Aβ aggregation is reported.

Experimental

Material and methods

All reagents were purchased as reagent grade from commercial suppliers and used without further purification unless otherwise specified. 2-Azidoethyl-4-methylbenzenesulfonate,[40] 1-azido-propanol (**1b**),[41] *tert*-butylazidoacetate (**1c**),[42] and 1-azido-5-amino-propane (**1d**)[43] were synthesized according to previously reported procedures. DCl and NaOD were purchased from Cambridge Isotope Laboratories. The $A\beta_{1-40}$ peptide was purchased from 21st Century Biochemicals (Marlborough, MA, USA). ^{1}H and ^{13}C NMR spectra were recorded on Bruker AV-500 or AV-600 instruments. Mass spectra (positive ion) were obtained on an Agilent 6210 time-of-flight electrospray ionization mass spectrometer. High resolution electrospray ionization mass spectrometry (HR-ESI(+)-MS) was performed at the Mass Spectrometry and Proteomics Facility at the University of Notre Dame. Electronic spectra were obtained on a Cary 5000 spectrophotometer. Turbidity assays were completed by measuring absorbance at 405 nm in a Synergy 4 Fluorometer

plate reader (BioTek). IR spectra were obtained using a Thermo Nicolet Nexus 670 FT-IR spectrometer at a 1 cm^{-1} resolution. Two-dimensional ^{1}H–^{15}N TROSY-HSQC (TROSY = transverse relaxation optimized spectroscopy; HSQC = heteronuclear single quantum correlation) nuclear magnetic resonance (NMR) spectra for the titration of **L1–L4** with ^{15}N-labeled $A\beta_{1-40}$ (rPeptide, Bogart, GA, USA) were recorded on a Bruker Avance 900 MHz spectrometer (Michigan State University).

Syntheses

4-(2-Azidoethyl)morpholine (1a). Morpholine (1.624 g, 18.7 mmol) and triethylamine (3.856 g, 38.1 mmol) were dissolved in 20 mL of CH_3CN. 2-Azidoethyl-4-methylbenzenesulfonate[40] (2.298 g, 9.5 mmol) was added and the solution gently refluxed for 4 days. The solvent was removed *in vacuo* and the residue was purified by silica gel chromatography (95 : 5 CH_2Cl_2/CH_3OH eluent) to afford **1a** as a yellow oil (1.471 g, 99%). ^{1}H NMR ($CDCl_3$, 400 MHz): δ 3.72 (t, J = 4.6 Hz, 4H), 3.35 (t, J = 5.9 Hz, 2H), 2.59 (t, J = 6.1 Hz, 2H), 2.50 (t, J = 4.6 Hz, 4H). FT-IR: 2963 cm^{-1} (w, sh), 2856 cm^{-1} (w, sh), 2810 (w, sh), 2100 (vs, sh), 1650 cm^{-1} (w, sh), 1452 cm^{-1} (w, sh), 1300 cm^{-1} (m, sh), 1117 cm^{-1} (vs, sh). ESI(+)-MS (m/z): $[M + H]^+$ Calcd for ($C_6H_{13}N_4O$), 157.10; Found, 157.11.

4-(2-(4-(Pyridin-2-yl)-1*H*-1,2,3-triazol-1-yl)ethyl)morpholine (L1). In a 20 mL vial, **1a** (0.504 g, 3.2 mmol) and 2-ethynylpyridine (0.364 g, 3.5 mmol) were dissolved in 1 mL of isopropanol. In a separate 20 mL vial, $CuSO_4{\cdot}5H_2O$ (0.041 g, 0.16 mmol) and L-ascorbic acid (0.290 g, 1.6 mmol) were dissolved in 2 mL of H_2O. Sonication was used to completely dissolve these components. The aqueous solution was added dropwise to the stirring isopropanol solution. The reaction was stirred for 2 h at 298 K and then Chelex resin was added to remove the Cu catalyst. The solution was filtered after 2 h to separate the Chelex resin and the solvent was removed *in vacuo*. The residue was purified by silica gel chromatography (95 : 5 CH_2Cl_2/CH_3OH eluent) to afford a pale yellow solid (0.584 g, 70% yield). ^{1}H NMR (D_2O, 600 MHz): δ 8.30 (d, J = 4.3 Hz, 1H), 8.15 (s, 1H), 7.72 (td, J = 7.8, 1.5 Hz, 1H), 7.65 (d, J = 7.9 Hz, 1H), 7.22 (ddd, J = 7.3, 5.2, 0.9 Hz, 1H), 4.51 (t, J = 7.0 Hz, 2H), 3.69 (t, J = 4.1 Hz, 4H), 2.86 (t, J = 7.0 Hz, 2H), 2.53 (t, J = 4.8 Hz, 4H). ^{13}C NMR (D_2O, 151 MHz): δ 148.24, 147.29, 146.18, 137.70, 123.27, 123.01, 120.01, 65.47, 56.24, 51.94, 46.35. HR-ESI(+)-MS (m/z): $[M + H]^+$ Calcd for ($C_{13}H_{18}N_5O$), 260.1511; found, 260.1506.

3-(4-(Pyridin-2-yl)-1*H*-1,2,3-triazol-1-yl)propan-1-ol (L2). In a 20 mL vial, **1b**[41] (0.205 g, 2.0 mmol) and 2-ethynylpyridine (0.207 g, 2.0 mmol) were dissolved in 1 mL of isopropanol. Employing reaction conditions identical to the synthesis of **L1** afforded a pale yellow solid, **L2** (0.290 g, 70% yield). ^{1}H NMR (D_2O, 600 MHz): δ 8.46 (s, 1H), 8.28 (s, 1H), 7.89 (td, J = 7.9, 1.6 Hz, 1H), 7.83 (d, J = 7.8 Hz, 1H), 7.38 (t, J = 6.2 Hz, 1H), 4.54 (t, J = 7.0 Hz, 2H), 3.62 (t, J = 6.2 Hz, 2H), 2.17 (t, J = 6.4 Hz, 2H). ^{13}C NMR (D_2O, 151 MHz): δ 148.17, 147.39, 146.07, 138.16, 123.44, 123.17, 120.41, 57.63, 46.95, 31.28. HR-ESI(+)-MS (m/z): $[M + H]^+$ Calcd for ($C_{10}H_{13}N_4O$), 205.1089; Found, 205.1084.

2-(4-(Pyridin-2-yl)-1*H*-1,2,3-triazol-1-yl)acetic acid (L3). In a 20 mL vial, **1c**[42] (0.489 g, 3.1 mmol) and 2-ethynylpyridine (0.322 g, 3.1 mmol) were dissolved in 1 mL of isopropanol. Employing reaction conditions identical to the synthesis of **L1** afforded a golden yellow solid. ^{1}H NMR ($CDCl_3$, 500 MHz): δ 8.59 (ddd, J = 6.1, 2.2, 1.2 Hz, 1H), 8.25 (s, 1H), 8.18 (dt, J = 9.9, 1.3 Hz, 1H), 7.80 (td, J = 9.6, 2.2 Hz, 1H), 7.23 (ddd, J = 9.4, 6.1, 1.5 Hz, 1H), 5.12 (s, 2H), 1.49 (s, 9H). All material produced in this step was dissolved in 15 mL of dichloromethane and 4.5 mL of trifluoroacetic acid (25 equiv.) was added and the reaction stirred overnight. The solvent was removed *in vacuo*, and multiple additions of diethyl ether induced precipitation of a pale yellow solid. This material was further purified by recrystallization from hot water to produce **L3** as white needles (0.611 g, 96% yield). ^{1}H NMR (D_2O, 600 MHz): δ 9.04 (s, 2H), 8.83 (td, J = 8.1, 1.6 Hz, 1H), 8.62 (dt, J = 8.2, 1.0 Hz, 1H), 8.21 (ddd, J = 7.6, 5.6, 1.2 Hz, 1H), 5.57 (s, 2H). ^{13}C NMR (D_2O, 151 MHz): δ 171.75, 145.55, 143.58, 142.63, 140.53, 126.97, 125.40, 123.74, 53.03. HR-ESI(+)-MS (m/z): $[M + H]^+$ Calcd for $[M + H]^+$ ($C_9H_9N_4O_2$), 205.0725; Found, 205.0720.

5-(4-(Pyridin-2-yl)-1*H*-1,2,3-triazol-1-yl)pentan-1-amine (L4). In a 20 mL vial, 1-azido-5-amino-propane,[43] **1d** (0.327 g, 2.5 mmol) and 2-ethynylpyridine (0.263 g, 2.5 mmol) were dissolved in 1 mL of isopropanol. Employing reaction conditions identical to the synthesis of **L1** afforded a residue that was purified by silica gel chromatography (1 : 1 CH_2Cl_2/CH_3OH with 1% NH_4OH eluent). Dissolving the residue in acidified CH_3OH and addition of diethyl ether precipitated **L4** as the hydrochloride salt (0.397 g, 67% yield). ^{1}H NMR (D_2O, 500 MHz): δ 8.24 (ddd, J = 6.2, 2.0, 1.1 Hz, 1H), 7.99 (s, 1H), 7.66 (td, J = 9.8, 2.2 Hz, 1H), 7.58 (dt, J = 9.9, 1.2 Hz, 1H), 7.15 (ddd, J = 9.3, 6.2, 1.6 Hz, 1H), 4.22 (t, J = 8.9 Hz, 2H), 2.48 (t, J = 9.0 Hz, 2H), 1.72 (quintet, J = 9.3 Hz, 2H), 1.33 (m, 2H), 1.15 (m, 2H). ^{13}C NMR (D_2O, 125 MHz): δ 148.65, 147.81, 146.65, 138.08, 123.62, 122.97, 120.32, 50.29, 40.21, 30.73, 29.13, 22.96. HR-ESI(+)-MS (m/z): $[M + H]^+$ Calcd for ($C_{12}H_{18}N_5$), 232.1562; Found, 232.1557.

Metal binding studies

Metal binding studies were performed by using a 50 μM ligand solution in a 1 : 1 ligand : metal ratio with either $CuCl_2$ or $ZnCl_2$ in CH_3CN. Ligand UV-vis spectra were first obtained, followed by addition of 20 μL of a 5 mM $CuCl_2$ or $ZnCl_2$ solution (1 equiv.) to the ligand solution to obtain UV-vis spectra of the metal complexes.

X-ray crystallography

Single crystals suitable for data collection were prepared by dissolving **L1** (0.027 g, 0.10 mmol) and $CuCl_2$ (0.018 g, 0.11 mmol), separately, in 0.5 mL of CH_3CN and then combining the solutions. Additional CH_3CN was added (*ca.* 5 mL) to increase solubility of the complex. The solution was sonicated and filtered. The solution was allowed to slowly evaporate to obtain greenish-blue crystals suitable for single crystal X-ray diffraction. **L3** (0.011 g, 0.05 mmol) and $Zn(NO_3)_2$ (0.016 g, 0.05 mmol) were first dissolved in 1 mL of CH_3CN and then 0.5 mL of H_2O was added to completely solubilize the metal–ligand complex. The solutions were filtered and allowed to slowly evaporate. The crystalline samples were mounted

on a 150 μm MiTeGen Dual-Thickness MicroMount using paraffin oil and data collected at room temperature. Crystallographic information can be found in Table 2. Disorder in C9/C10 for the Cu complex was modelled with floating occupancies to 0.752/0.248. All diffraction data were processed with the Bruker Apex II software suite. The structures were solved with SIR92 and subsequent refinements were performed using CRYSTALS.[44] Diagrams were prepared using ORTEP-3[45] and POV-RAY.[46]

Determination of acidity constants by UV-vis

In order to determine the speciation of **L1–L4** at physiological pH, acidity constants were measured by obtaining variable pH UV-vis spectra. Solutions of **L1–L4** (50 μM) were prepared in 0.1 M PBS buffer at pH 6.6. Before obtaining UV-vis spectra, a pH electrode was calibrated using a 2-point method (pH 4.01 and pH 10.01 standard buffers). NaOH was used to increase the pH of the ligand solutions to a starting point of *ca.* pH 12. Aliquots of HCl were added to the **L1–L4** ligand solution and UV-vis spectra obtained in the range of 600–190 nm. At least 30 UV-vis spectra were obtained in the range of pH 2–12. Spectral data was analyzed using the HypSpec program (Protonic Software, UK).[47] Speciation diagrams for **L1–L4** were simulated using the HySS2009 program (Protonic Software, UK).[48]

Determination of acidity constants by NMR

For pK_a values that could not be measured using UV-vis spectroscopy, variable pH NMR experiments were performed in order to follow changes in chemical shifts based on individual protonation sites of **L1–L4**. Solutions of 80–100 mg **L1–L4** in 8 mL of D_2O were prepared. NaOD and DCl were used to vary the pD of the solution. Before NMR aliquots were prepared, a pH electrode was calibrated using a 2-point method (pH 4.01 and pH 10.01 standard buffers). Once the pH of the solution had stabilized, 500 μL of solution was obtained and placed in an NMR tube. Ten aliquots were prepared and ^{1}H and/or ^{13}C experiments were run on a Bruker AVANCE III 500 MHz NMR or a Bruker AVANCE II 600 MHz NMR. Chemical shifts for the *o*-H to the pyridine N and the triazole H were used to determine the pK_a for the chelation site. Depending on the R-group, the pK_a was determined by measuring the chemical shifts of the protons in the vicinity of the protonation site over a specific pH range. NMR data was analyzed by HypNMR (Protonic Software, UK). Speciation diagrams for **L1–L4** were simulated using the HySS2009 program (Protonic Software, UK). The equation (pK_a (H_2O) = (pK_a (D_2O) −0.45)/1.015) was used to convert pD values to pH values.[49]

Two-dimensional (2D) ^{1}H–^{15}N transverse relaxation optimized spectroscopy (TROSY)-heteronuclear single quantum correlation (HSQC) NMR measurements

A *ca.* 308 μM solution of ^{15}N-labeled Aβ_{1-40} (rPeptide, Bogart, GA, USA) was prepared from *ca.* 0.25 mg of peptide dissolved in 186 μL of an aqueous buffer containing SDS-d_{25} (200 mM), NaPi (20 mM, pH 7.3), and D_2O (7%, v/v). Spectra of the peptide solutions were acquired in a Shigemi NMR tube at 298 K. The ligands **L1–L4** were added to the peptide solution from a stock solution in the above buffer (5 mM) to give 1, 5, and 10 equivalents of ligand to peptide. Two-dimensional ^{1}H–^{15}N HSQC spectra were collected at 298 K, with spectral widths of 14.3 kHz (^{1}H) and 1.7 KHz (^{15}N), using 4 transients per free-induction decay, 128 complex points in the ^{15}N dimension, and 2048 complex points in the ^{1}H dimension. Total experiment time for each spectrum was 10 min.[50–53] The water peak was referenced to 4.77 ppm at 298 K. ^{1}H–^{15}N HSQC peaks were assigned by comparison of the observed chemical shift values to those reported in the literature.[54] Combined backbone ^{1}H and ^{15}N 2D chemical shifts were calculated using eqn (1).[55] 2D spectra were processed using Topspin software (version 2.1) from Bruker and analyzed with Sparky (version 3.112).

$$\Delta\delta_{N-H} = \sqrt{\frac{(\Delta\delta_H)^2 + (0.2(\Delta\delta_N))^2}{2}} \quad (1)$$

Docking studies using AutoDock Vina

Potential molecular conformations of the ligands with Aβ_{1-40} were elucidated *in silico* using AutoDock Vina,[56] AutoDock-Tools4,[57] and PyRx.[58] The 2D structures of **L1–L4** were generated in MarvinSketch (ChemAxon, Budapest, Hungary), and the corresponding lowest energy conformations were obtained using ChemAxon's chemical calculators. The predicted major microspecies for **L3** at pH 7.3 were generated using the same calculators. The SDS condition receptor was obtained from the PDB (1BA4)[59] from an NMR-derived Aβ_{1-40} structure in SDS-d_{25} micelles; all 10 conformations were used for docking. Docking was performed using AutoDock Vina through the PyRx suite. Search space for each receptor conformation was set to the bounds of the peptide and an exhaustiveness of 1024 was used. Docked poses were viewed using Pymol, after which the conformations that best represented the experimental conditions were chosen based on the relative proximity (<5 Å) of ligand heavy atoms to the majority of perturbed amino acid residues.[60]

Turbidity measurements

Lyophilized synthetic human Aβ_{1-40} (21st Century Biochemicals) was freshly prepared as a 200 μM stock solution before each trial was performed. Each vial of peptide contained 0.25 mg Aβ_{1-40}, which was dissolved in 290 μL of deionized water. To achieve complete dissolution of the peptide, sonication for 1 minute followed by a 30 second pause was repeated twice. Chelex-treated 20 mM HEPES buffer containing 150 mM NaCl was prepared in deionized water at pH 6.6 and 7.4 for both Cu and Zn turbidity assays, respectively, and used to prepare stock solutions of ligands, metals, and ascorbate, as well as the reaction mixtures in the 96-well plates. Each ligand measurement was evaluated in quadruplicate. Ligands, metals, and Aβ_{1-40} peptide had final concentrations of 150 μM, 25 μM, and 25 μM, respectively, in the turbidity assay. Cu and Zn solutions were prepared from atomic absorption standards (Sigma-Aldrich). Turbidity assays were completed in flat-bottomed 96-well assay plates (Microtest, BD Falcon). Metal, Aβ_{1-40}, and HEPES buffer were first added to the 96-well plate followed by the ligands. After a 45 minute incubation period in a 37 °C water bath under constant agitation, each well in the 96-well plate was measured at 405 nm using a Synergy 4 Fluorometer plate reader from BioTek. Blanks containing ligand, metal, and buffer were also measured and subtracted from corresponding wells. Wells containing metal

and peptide were used as a positive control to demonstrate amount of aggregation in the absence of ligand.

Transmission electron microscopy (TEM)

Samples were prepared by incubating the Aβ peptide (25 μM) with and without $CuCl_2$ or $ZnCl_2$ (25 μM) and **L1** (50 μM) for 24 hours in a 37 °C water bath. TEM grids were prepared following previously reported methods.[61] Formvar/Carbon 300-mesh grids (Electron Microscopy Sciences) were glow-discharged in air for 15 seconds to increase hydrophilicity. Samples (10 μL) were dropped onto a sheet of parafilm and the TEM grid was placed on the drop for 5 minutes. Afterward, the grid was stained with syringe-filtered 5% uranyl acetate from 3 × 30 μL drops placed onto parafilm. The grid was placed on the first drop of uranyl acetate and immediately removed, repeated for the second drop, then placed on the third drop to incubate for 1 minute. Excess uranyl acetate was removed using a tissue between drops. The grid was allowed to air-dry for at least 15 minutes. Bright field images were obtained at 200 kV and 9000× magnification.

Results and discussion

Design and synthesis of TriPy ligands

The development of compounds capable of metal binding as well as inhibiting Aβ aggregation is of considerable interest for AD research. The synthesis of a small library of triazole–pyridine ligands **L1–L4** (Fig. 2) was completed using a facile Cu-catalyzed alkyne–azide cycloaddition reaction of 2-ethynylpyridine with a number of different azide fragments (Scheme 1). Click chemistry allows for the modular synthesis of a number of TriPy ligands with an identical bidentate metal binding function, while varying the peripheral R-group. This synthetic pathway permitted the rapid development of a series of metal-binding compounds for study in disease-relevant assays. Four azides containing different functional groups (R) were synthesized,[40–43] and each azide was coupled with 2-ethynylpyridine *via* click chemistry (Scheme 1).[36,62] To complete the synthesis of **L3**, trifluoroacetic acid was used to remove the ^{t}Bu group and afford the free carboxylic acid. The synthetic route described allows for the synthesis of **L1–L4** in two to three steps in good to excellent yields (Scheme 1).

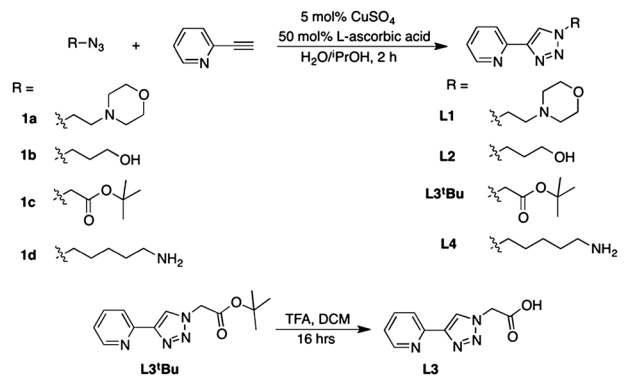

Scheme 1 Synthetic routes for the preparation of **L1–L4**.

Ligand speciation measurements

To determine the solution speciation of **L1–L4**, variable pH UV-vis (Fig. 3 and Fig. S1–S3, ESI‡), and ^{1}H NMR (Fig. S4–S8, ESI‡) experiments were performed in the pH 2–12 range. As shown in Fig. 3, **L2** contains only one protonated species in the pH range studied, which corresponds to the triazole–pyridine unit as protonation clearly affects the π–π* transition of the conjugated ring system. Fitting the variable pH UV-vis data for **L2** affords a single pK_a value of 3.40(6) (Table 1). This pK_a value is lower than the pK_a of pyridine (pK_a = 5.25),[63] and that of 2,2′-bipyridine (pK_a = 4.30),[64] and it is possible that hydrogen bonding stabilizes a *trans* geometry of the pyridine-N and triazole-N thus lowering the pK_a value for the TriPy ligands relative to pyridine. The low pK_a value for the pyridine–triazole unit (uncharged at physiological pH) is potentially important for biological uptake of this class of compounds. The variable pH UV-vis spectra of **L1**, **L3**, and **L4** exhibit similar pK_a values in comparison to **L2** for the pyridyl nitrogen (Table 1).

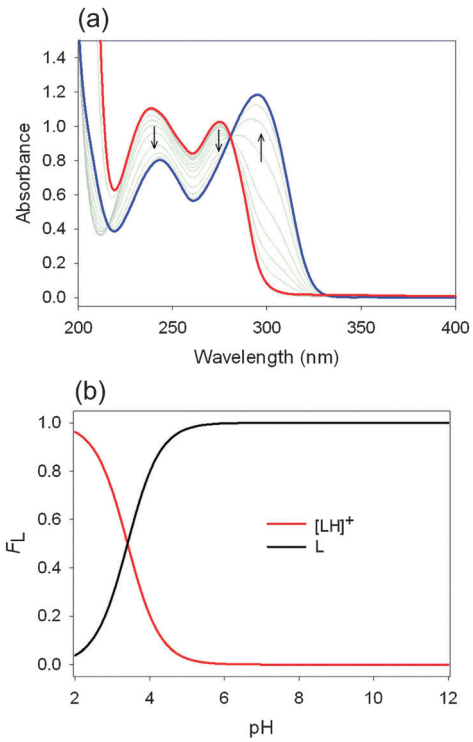

Fig. 3 Solution speciation studies of **L2**. (a) Variable-pH UV-vis spectra of **L2** (pH range 2–12; [**L2**] = 50 μM). (b) Solution speciation diagram for **L2**.

Table 1 pK_a values and speciation at physiological pH as determined by UV-vis and NMR spectroscopy

	UV-vis	NMR		
	pK_a (TriPy)	pK_a (TriPy)	pK_a (R-group)	Speciation (pH 7.4)
L1	3.05(1)	2.84(8)	4.89(3)	Neutral
L2	3.40(6)	3.31(7)	n/a	Neutral
L3	3.45(7)	3.08(7)	2.3(1)	Monoanionic
L4	3.21(9)	3.15(5)	10.3(3)	Monocationic

Table 2 Crystallographic data for [Cu(**L1**)Cl_2] and [Zn(**L3**)$(NO_3)_2(H_2O)$]

	[Cu(**L1**)Cl_2]	[Zn(**L3**)$(NO_3)_2(H_2O)$]
Formula	$C_{13}H_{17}Cl_2CuN_5O$	$C_9H_{10}N_6O_9Zn$
F_w	393.76	411.59
Crystal system	Monoclinic	Triclinic
Space group	$P2_1/n$	$P\bar{1}$
a (Å)	12.4564(3)	7.1753(3)
b (Å)	8.7526(2)	9.9395(4)
c (Å)	14.9349(4)	11.0467(5)
α (°)	—	75.271(3)
β (°)	96.602(2)	74.091(3)
γ (°)	—	80.029(3)
V (Å^3)	1617.49(7)	728.22(6)
Z	4	2
Temp. (K)	296(2)	296(2)
ρ_{calcd} (g cm^{-3})	1.617	1.877
θ limits (°)	2.33, 28.07	2.97, 28.15
μ (Mo Kα) (mm^{-1})	1.688	1.752
Reflections	13 351	9606
Unique	3925	3484
No. of params	223	235
GOF[a]	1.1370	1.1068
A_i	0.262, 0.294, 0.103	0.152, 0.0798, 0.0427
R_1[b]	0.0506	0.0314
wR_2[c]	0.0501	0.0316

[a] [Weight] = $1.0/[A_0 \times T_0(x) + A_1 \times T_1(x) \cdots + A_{n-1}] \times T_{n-1}(x)]$ where A_i are the Chebychev coefficients listed above and $x = F_{calc}/F_{max}$ and using the method of Robust Weighting W = [weight] $\times [1 - (\Delta F/6 \times \sigma F)^2]^2$. [b] $R = \Sigma||F_o| - |F_c||/\Sigma|F_o|$. [c] $wR^2 = \{\Sigma[w(F_o^2 - F_c^2)^2]/\Sigma[w(F_o^2)^2]\}^{1/2}$.

To obtain a more complete understanding of the speciation of **L1–L4** at physiological pH, variable pH ^{1}H NMR spectra were obtained. Chemicals shifts of protons in the vicinity of a potential protonation site were monitored, and based on the fitted NMR data, **L2** was determined to exhibit a single pK_a (3.31(7)), in agreement with the UV-vis data (Fig. S5, ESI‡). Thus, at physiological pH (pH 7.4), **L2** was determined to be a neutral species in aqueous solution. Fitting the variable pH NMR chemical shifts of **L1** allows for the determination of the morpholine pK_a value (Table 1 and Fig. S6, ESI‡). Using NMR, the pK_a of the morpholine amine was determined to be 4.89(3), while the pK_a of the pyridine unit was 2.84(8). The pK_a values for morpholine (8.36) and *N*-methylmorpholine (7.38)[65] are higher than the value determined for **L1**, which could be due to steric and/or electronic effects of the triazole–pyridine ring system.[66] Based on the NMR data, **L1** is also expected to be a neutral compound at physiological pH. The pyridine pK_a (2.84(8)) is slightly lower in comparison to that of **L2**, likely due to the protonated morpholine function, and this value coincides well with UV-vis analysis (Table 1). The carboxylic acid moiety of **L3** is expected to be deprotonated at physiological pH, and the variable pH NMR spectra confirm two pK_a values at 2.3(1) and 3.08(7). By analysis of the UV-vis and NMR (Fig. S2 and S7, ESI‡) data the former pK_a is assigned to the carboxylic acid and the latter pK_a to the pyridine unit, and thus at physiological pH **L3** is a monoanionic species. The variable pH NMR data of **L4** (Fig. S8, ESI‡) can be fit to a pK_a value of 10.3(3), indicating that **L4** exists as a monocation at pH 7.4 (*via* protonation of the primary amine). The peripheral R-groups thus afford us the opportunity to investigate how charge influences the interactions of **L1–L4** with the Aβ peptide under physiological conditions. In addition, the solution speciation results show that the bidentate triazole–pyridine binding unit is neutral at physiological pH, which may be beneficial for *in vivo* applications.

Metal binding properties

The interactions of **L1–L4** with Cu(II) and Zn(II) ions were probed using UV-vis spectroscopy and X-ray crystallography. Upon addition of metal ions to solutions of ligand, increased intensity and shifts of the optical bands at *ca.* 235 nm and 275 nm were observed relative to **L1** (Fig. 4). Similar shifts of these peaks for **L2–L4** (Fig. S9–S11, ESI‡) were also observed upon treatment with metal ions indicating interaction of the bidentate metal-binding unit with Cu(II) and Zn(II) in each case. Addition of a $CuCl_2$ solution afforded additional weak bands at *ca.* 390 nm and 460 nm. The change in intensity of the ligand-based transitions, along with the observation of new optical bands at *ca.* 390 nm and 460 nm indicated metal binding to ligands **L1–L4**.

The metal-binding properties of **L1** and **L3** were further explored by X-ray crystallography. Crystals were obtained by slow evaporation of a solution of 1 : 1 ligand to metal in CH_3CN and/or H_2O. Single crystals of [Cu(**L1**)Cl_2] were produced by slow evaporation from CH_3CN. Fig. 5 shows the metal complex, with **L1** bound to the Cu centre in a bidentate fashion using two nitrogen atom donors, one from pyridine and the other from the triazole ring with two additional chloride ligands present. Additional weak axial interactions to the Cu(II) centre exist from a neighbouring chloride ligand and a morpholine oxygen atom (Fig. S12, ESI‡). **L1** exists in a flat, planar geometry in the crystal structure. In addition to the Cu(**L1**) complex, single crystals of [Zn(**L3**)$(NO_3)_2(H_2O)$] were obtained by slow evaporation of a 1 : 1 mixture of **L3** and $Zn(NO_3)_2$ in CH_3CN/H_2O. A similar bidentate coordination to Zn(II) was observed for **L3** where two nitrogen donor atoms from pyridine and the triazole, respectively, are coordinated to the centre of Zn(II) (Fig. 6). Taken together, the X-ray structures along with UV-vis data supports metal binding of **L1–L4** to Cu(II) and Zn(II).

NMR studies for ligand–peptide interactions

Experiments using 2D ^{1}H–^{15}N TROSY-HSQC NMR spectroscopy were employed in order to investigate the interactions of **L1–L4** with metal-free $A\beta_{1-40}$ monomer in the presence sodium

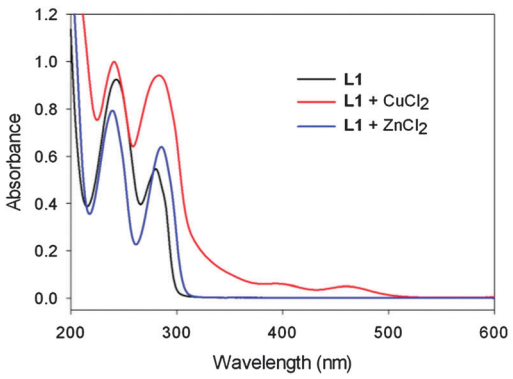

Fig. 4 UV-vis spectra of **L1** (50 μM, black) incubated with metal ions (50 μM) in CH_3CN (**L1** + $CuCl_2$ (red), **L1** + $ZnCl_2$ (blue)).

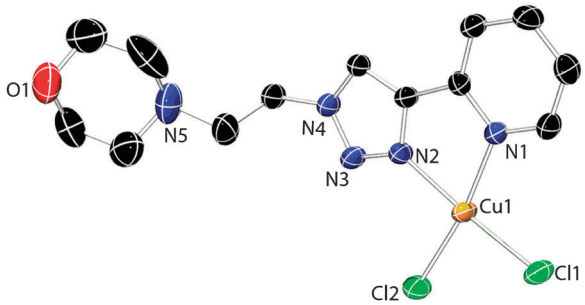

Fig. 5 ORTEP diagram of [Cu(**L1**)Cl_2] showing 50% probability thermal ellipsoids. Selected bond lengths (Å) and angles (deg): Cu(1)–N(1) = 2.062(2); Cu(1)–N(2) = 2.024(3); Cu(1)–Cl(1) = 2.2647(8); Cu(1)–Cl(2) = 2.2417(9); Cu(1)–O(1) = 2.808(3); N(1)–Cu(1)–N(2) = 79.31(10); Cl(1)–Cu(1)–N(1) = 86.80(8); N(2)–Cu(1)–Cl(2) = 92.32(7); Cu(1)–Cl(1)–Cu(2) = 94.86(3); Cl(1)–Cu(1)–O(1) = 163.22(8).

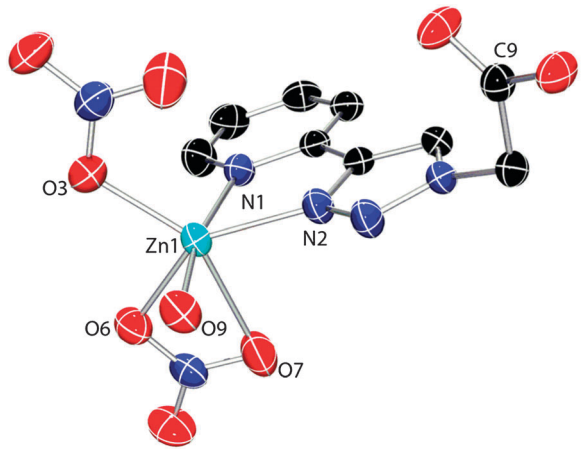

Fig. 6 ORTEP diagram of [Zn(**L3**)$(NO_3)_2(H_2O)$] showing 50% probability thermal ellipsoids. Selected bond lengths (Å) and angles (deg): Zn(1)–O(3) = 2.0348(19); Zn(1)–O(6) = 2.0864(18); Zn(1)–O(7) = 2.503(2); Zn(1)–O(9) = 2.1036(19); Zn(1)–N(1) = 2.174(2); Zn(1)–N(2) = 2.0749(19); O(3)–Zn(1)–O(6) = 88.49(8); O(3)–Zn(1)–O(7) = 142.21(8); O(6)–Zn(1)–O(7) = 54.70(7); O(3)–Zn(1)–O(9) = 95.61(8); O(6)–Zn(1)–O(9) = 92.02(7); N(1)–Zn(1)–N(2) = 76.36(7); O(3)–Zn(1)–N(2) = 129.71(8); O(7)–Zn(1)–N(2) = 86.56(7); O(9)–Zn(1)–N(1) = 166.67(7).

dodecyl sulfate-d_{25} (SDS-d_{25}). Previous structural studies have used detergent micelles as a model membrane and also to trap the helical intermediates present in the misfolding pathway. It was shown that $A\beta_{1-40}$ embedded in SDS micelles is monomeric with residues 15 to 36 forming an α-helix with a kink from residues 25 to 27, and the N-terminal residues 1 to 14 are unstructured.[54,59,67] In the presence of SDS, the introduction of **L1–L4** (1, 5, and 10 equiv.) into the buffered solution (pH 7.3) of monomeric $A\beta_{1-40}$ induced changes in chemical shifts in the ^1H–^{15}N TROSY-HSQC spectrum of the peptide, particularly in the region between E3 and E22 (Fig. 7 and Fig. S13, ESI‡). In particular, upon addition of 10 equiv. of **L1**, significant chemical shift perturbations were observed for the amino acid residues E11, H13, and Q15 (Fig. 7). These residues are in close proximity to the proposed metal chelating site in $A\beta_{1-40}$, which may involve three His residues

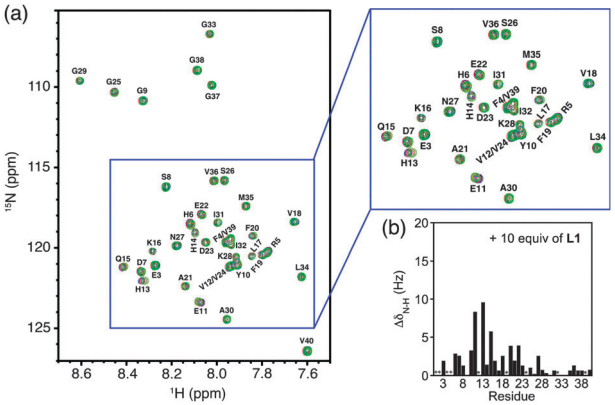

Fig. 7 NMR studies of **L1** against ^{15}N-labeled $A\beta_{1-40}$ in the SDS condition. (a) 2D ^1H–^{15}N TROSY-HSQC NMR spectra of **L1** (0, 1, 5, and 10 equiv., indicated by black, blue, red, and green, respectively) with the peptide (200 mM SDS-d_{25}, 20 mM NaPi, pH 7.3, 7% v/v D_2O). (b) Calculated ^1H and ^{15}N chemical shifts of $A\beta_{1-40}$ in the presence of 10 equivalents of **L1**. Peaks that could not be resolved due to overlap or absence are indicated by an asterisk (*).

(*i.e.*, H6, H13, and H14).[3,51] This suggests that **L1** has the potential to interact with Aβ monomer near the proposed metal binding site and perturb the metal-mediated peptide aggregation.[51–53] **L2–L4** also displayed changes in chemical shifts of amino acid residues in the vicinity of the metal binding site of the peptide, but the shifts were smaller in comparison to **L1** (Fig. S13, ESI‡). In the case of **L3** (Fig. S13b, ESI‡), several additional peaks in the HSQC spectrum shift as a result of treatment with 10 equiv. of the ligand; however, the direction of the shift for residues E11, H13, Q15, F20, and E22 upon titrating with **L3** is in opposition to that observed for the corresponding residues while titrating with the ligands **L1**, **L2**, and **L4**.

Due to the low pK_a of the carboxylic acid moiety of **L3**, the ligand at 10 equivalents it may sufficiently lower the pH of the peptide solution leading to the observed spectral changes; thus, it would be a challenge to fully attribute the spectral changes to **L3**. The $A\beta_{1-40}$ monomer has been shown to exhibit a more structured conformation upon decreasing pH in the presence of SDS (with the helical structure near residues 15–24 being especially sensitive to changes in pH).[59,68] NMR titration experiments under the SDS conditions show that all ligands affected residues near the purported metal binding site in $A\beta_{1-40}$, with **L1** inducing the largest chemical shift changes in amino acid residues.

Docking studies

To better understand and visualize the interactions of **L1–L4** with the monomeric Aβ peptide, the small molecules were docked against the previously reported NMR structure of monomeric $A\beta_{1-40}$ (PDB 1BA4)[59] in the presence of SDS micelles using AutoDock Vina (Fig. 8 and Fig. S14, ESI‡).[56] Due to imperfections in scoring functions and limited ability to cope with the dynamic nature of protein–ligand interactions,[69] multiple receptors (NMR ensembles) were used to account for some level of dynamics in the $A\beta_{1-40}$ monomer. Ligand poses generated by AutoDock Vina were ranked according to predicted binding affinities (Table S1, ESI‡).[70] Of these results,

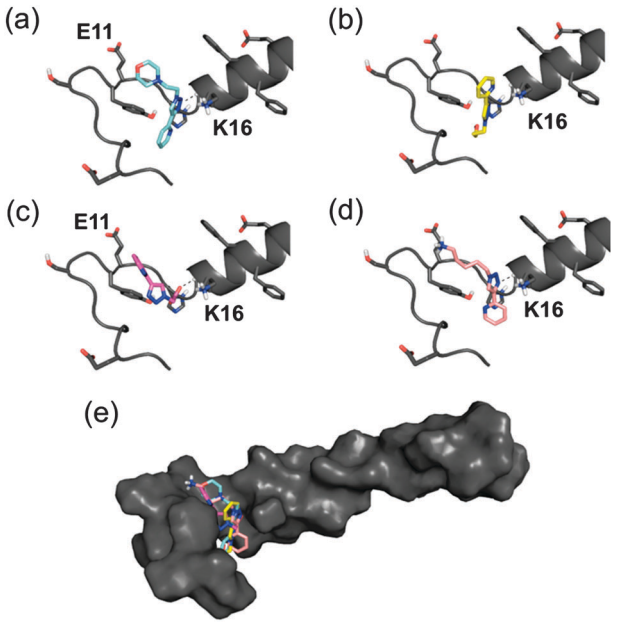

Fig. 8 Docking of small molecules with $A\beta_{1-40}$ monomer in the presence of SDS (PDB 1BA4)[59] predicted by AutoDock Vina. Cartoon depictions of (a) **L1** (light blue), (b) **L2** (yellow), (c) **L3** (carboxylate form, magenta), and (d) **L4** (protonated form, light pink) with $A\beta_{1-40}$ in the presence of SDS (PDB 1BA4) in Conformation A. Surface depiction of **L1–L4** interacting with $A\beta_{1-40}$ (e).

four poses using SDS conditions that supported the observations from NMR experiments (*vide supra*) were selected as representative theoretical bound conformations (Fig. 8 and Fig. S14, ESI‡). Poses that best represented the experimental conditions were chosen based on the relative proximity (< 5 Å) of ligand heavy atoms to the majority of perturbed amino acid residues.[60] Similar poses were predicted for each ligand among the various peptide conformations (Fig. 8 and Fig. S14, ESI‡). Docking results suggest that the ligands favour the N-terminal region, clustering near residues E11, Q15, and the putative metal binding site (H6, H13, and H14).[3,51,52] Potential non-covalent interactions were identified between the small molecules and the nearby residues that NMR results indicated were likely sensitive to the introduction of ligands. For both **L1** and **L4**, the triazole ring is predicted to interact with the K16 residue, while **L2** and **L3** are predicted to interact near the metal binding site in the opposite orientation. The ligands are likely fluxional in solution (*N*,*N cis* and *N*,*N trans*) and thus both conformations could interact with the Aβ peptide. Interestingly, the triazole nitrogen, and not the pyridine nitrogen, is predicted to interact with the peptide. Overall, these theoretical poses suggest the interaction of **L1–L4** with monomeric Aβ species.

Inhibition of Aβ aggregation

Previous reports have demonstrated that the interaction of Cu(II) and Zn(II) with the Aβ peptide facilitates aggregation.[19,23,71] Interestingly, metal binding agents could disrupt metal-induced Aβ aggregation *via* chelation, thus limiting Aβ fibril formation.[32,72] In this work, a turbidity assay *via* light scattering measurements (405 nm) was first used to study the ability of **L1–L4** to regulate metal-induced aggregation of the Aβ peptide (Fig. 9). This assay provides information about the degree of peptide aggregation in bulk solution. The lower pH value for Cu(II) was chosen as Cu(II)-induced aggregation is optimal at pH 6.6.[73] The high affinity metal ion chelator, diethylenetriaminepentaacetic acid (DTPA),[74] is used as a positive control, and demonstrates essentially complete inhibition of both Cu(II)- and Zn(II)-induced aggregation in this study. **L1–L4** were shown to inhibit Cu(II)- and Zn(II)-induced Aβ aggregation by 50–90% at pH 6.6 and 7.4, respectively (Fig. 9). Secondly, to further demonstrate that **L1** is able to influence metal-induced Aβ aggregation, analysis of the samples containing metal ions, Aβ, and **L1** was conducted by transmission electron microscopy (TEM). As shown in Fig. 10, upon incubating the Aβ peptide with either $CuCl_2$ or $ZnCl_2$, a significant amount of fibrillogenesis is observed. When the ligand **L1** was introduced to a metal–peptide solution before incubation, smaller and fewer aggregates were observed after 24 h. This further supports the hypothesis that **L1** could alter metal-induced Aβ peptide aggregation.

It is possible that by limiting aggregation, oligomeric species are produced.[13] While this needs to be studied further, by contributing to the break-up of Aβ plaque deposits, small-molecule chelators also increase the local concentration of metal ions as well as the Aβ peptide. Interestingly, an increase in metal concentration was found to up-regulate matrix metalloproteases MMP-2 and MMP-3, leading to a more rapid degradation of the Aβ peptide.[75] Further studies have shown that increasing Cu bioavailability activates neuroprotective cell signaling pathways, most importantly the inhibition of glycogen synthase kinase 3β (GSK3β).[76] Inhibition of GSK3β *in vitro* was found to increase expression of Aβ-degrading proteases.[75] Aβ oligomers are not always toxic, and in certain cases unstructured amorphous species have been suggested to be non-toxic.[77] The toxicity of the Aβ species generated in these conditions has yet to be quantified.

We also investigated the ability of **L1** to influence Aβ peptide aggregation in the absence of metal ions. Incubation of Aβ peptide for 24 h leads to fibril formation (Fig. 11), albeit

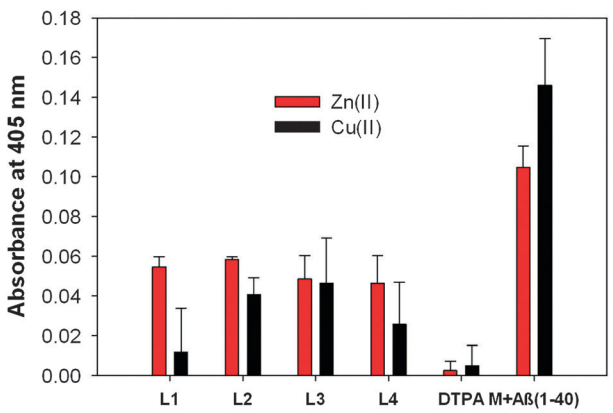

Fig. 9 Degree of $A\beta_{1-40}$ aggregation as measured by UV-vis measurements. Data represents the mean absorbance of quadruplicate trials at 405 nm of peptide in the presence of metal ions and ligands at pH 6.6 and 7.4 for Cu(II) and Zn(II), respectively. Error bars represent the standard deviation of the average absorbance value. See experimental section for details.

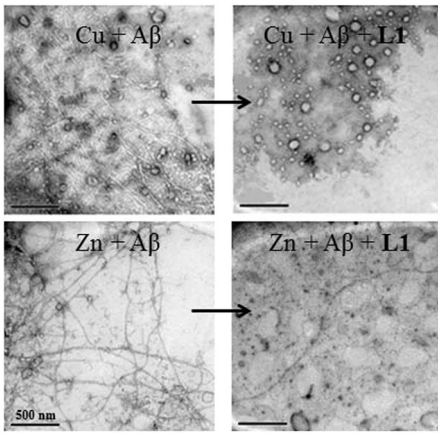

Fig. 10 TEM images of samples incubated with 25 μM $A\beta_{1-40}$, 25 μM metal ions, and 50 μM **L1** were incubated for 24 h at 37 °C. Top: TEM images of $A\beta_{1-40}$ + $CuCl_2$, (left); $A\beta_{1-40}$ + $CuCl_2$ + **L1** (right). Bottom: $A\beta_{1-40}$ + $ZnCl_2$ (left); $A\beta_{1-40}$ + $ZnCl_2$ + **L1** (right).

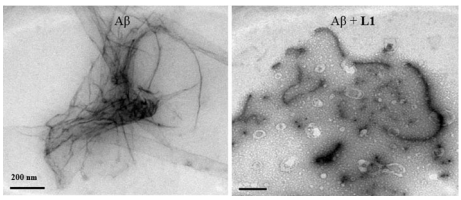

Fig. 11 TEM images of the samples containing metal-free $A\beta_{1-40}$ species (25 μM) and **L1** (50 μM). TEM images of metal-free $A\beta_{1-40}$ species (left) and of metal-free $A\beta_{1-40}$ species treated with **L1** (right) (conditions: 24 h at 37 °C).

fibril morphology is smaller and thinner in comparison to Aβ exposed to $CuCl_2$ or $ZnCl_2$. Incubation of the Aβ peptide with **L1** leads to a mixture of fibrillar and unstructured aggregates in comparison to the peptide alone (Fig. 11). The overall results from studies of both metal-free and metal-induced Aβ aggregation employing **L1** suggest that **L1** could interact with Aβ peptides (along with 2D NMR studies, *vide supra*) and may restrict the formation of Aβ fibrils in both the absence and presence of metal ions.

Summary

Four bifunctional ligands **L1–L4** containing a triazole–pyridine metal binding scaffold were prepared and studied. The compounds were assembled in a modular fashion using click chemistry to afford a uniform metal-binding unit, while allowing for the installation of different peripheral groups. The protonation states and metal binding properties of **L1–L4** were investigated by UV-vis, NMR, and/or X-ray crystallography. Subsequent 2D NMR investigations and docking studies provided important information on the ability of **L1–L4** to interact directly with the metal-free Aβ peptide in solution. Turbidity and TEM studies demonstrated their ability to inhibit Aβ aggregation processes in the presence of metal ions. All four ligands were found to influence metal-induced Aβ aggregation, with **L1** considered to be the most promising bifunctional molecule. Overall, the TriPy ligand framework shows promise for disrupting metal–Aβ interactions and peptide aggregation.

Acknowledgements

This work is supported by an NSERC Discovery Grant (to T.S.) and the Alzheimer's Association (NIRG-10-172326) (to M.H.L.). We also thank the Alzheimer Society of Canada for a doctoral award and Simon Fraser University for a Graduate Fellowship (to M.R.J.) and the National Science Foundation (to A.S.D.) for a Graduate Research Fellowship.

Notes and references

1 V. H. Finder, *J. Alzheimers Dis.*, 2010, **22**, S5–S19.
2 K. J. Barnham, C. L. Masters and A. I. Bush, *Nat. Rev. Drug Discovery*, 2004, **3**, 205–214.
3 E. Gaggelli, H. Kozlowski, D. Valensin and G. Valensin, *Chem. Rev.*, 2006, **106**, 1995–2044.
4 A. S. DeToma, S. Salamekh, A. Ramamoorthy and M. H. Lim, *Chem. Soc. Rev.*, 2012, **41**, 608–621.
5 (*a*) www.alzheimer.ca; (*b*) www.alz.org.
6 (*a*) E. D. Roberson and L. Mucke, *Science*, 2006, **314**, 781–784; (*b*) P. A. Adlard, S. A. James, A. I. Bush and C. L. Masters, *Drugs Today*, 2009, **45**, 293–304; (*c*) M. Citron, *Nat. Rev. Drug Discovery*, 2010, **9**, 387–398.
7 D. J. Selkoe, *Nat. Med.*, 2011, **17**, 1693–1695.
8 K. Sambamurti, N. H. Greig and D. K. Lahiri, *Neuromol. Med.*, 2002, **1**, 1–31.
9 (*a*) G. K.-W. Kong, J. J. Adams, H. H. Harris, J. F. Boas, C. C. Curtain, D. Galatis, C. L. Masters, K. J. Barnham, W. J. McKinstry, R. Cappai and M. W. Parker, *J. Mol. Biol.*, 2007, **367**, 148–161; (*b*) J. A. Duce, A. Tsatsanis, M. A. Cater, S. A. James, E. Robb, K. Wikhe, S. L. Leong, K. Perez, T. Johanssen, M. A. Greenough, H.-H. Cho, D. Galatis, R. D. Moir, C. L. Masters, C. McLean, R. E. Tanzi, R. Cappai, K. J. Barnham, G. D. Ciccotosto, J. T. Rogers and A. I. Bush, *Cell*, 2010, **142**, 857–867.
10 D. J. Selkoe and D. Schenk, *Annu. Rev. Pharmacol. Toxicol.*, 2003, **43**, 545–584.
11 C. A. McLean, R. A. Cherny, F. W. Fraser, S. J. Fuller, M. J. Smith, K. Beyreuther, A. I. Bush and C. L. Masters, *Ann. Neurol.*, 1999, **46**, 860–866.
12 (*a*) A. Abbott, *Nature*, 2008, **456**, 161–164; (*b*) J. Hardy and D. J. Selkoe, *Science*, 2002, **297**, 353–356.
13 S. Lesné, M. T. Koh, L. Kotilinek, R. Kayed, C. G. Glabe, A. Yang, M. Gallagher and K. H. Ashe, *Nature*, 2006, **440**, 352–357.
14 M. A. Busche, G. Eichhoff, H. Adelsberger, D. Abramowski, K.-H. Wiederhold, C. Haass, M. Staufenbiel, A. Konnerth and O. Garaschuk, *Science*, 2008, **321**, 1686–1689.
15 P. E. Cramer, J. R. Cirrito, D. W. Wesson, C. Y. D. Lee, J. C. Karlo, A. E. Zinn, B. T. Casali, J. L. Restivo, W. D. Goebel, M. J. James, K. R. Brunden, D. A. Wilson and G. E. Landreth, *Science*, 2012, **335**, 1503–1506.
16 (*a*) I.-T. Hsiao, C.-C. Huang, C.-J. Hsieh, W.-C. Hsu, S.-P. Wey, T.-C. Yen, M.-P. Kung and K.-J. Lin, *Eur. J. Nucl. Med. Mol. Imaging*, 2012, **39**, 613–620; (*b*) A. D. Joshi, M. J. Pontecorvo, C. M. Clark, A. P. Carpenter, D. L. Jennings, C. H. Sadowsky, L. P. Adler, K. D. Kovnat, J. P. Seibyl, A. Arora, K. Saha, J. D. Burns, M. J. Lowrey, M. A. Mintun and D. M. Skovronsky, *J. Nucl. Med.*, 2012, **53**, 378–384.
17 (*a*) A. Nunomura, G. Perry, G. Aliev, K. Hirai, A. Takeda, E. K. Balraj, P. K. Jones, H. Ghanbari, T. Wataya, S. Shimohama, S. Chiba, C. S. Atwood, R. B. Petersen and M. A. Smith, *J. Neuropathol. Exp. Neurol.*, 2001, **60**, 759–767; (*b*) D.-H. Cho, T. Nakamura, J. Fang, P. Cieplak, A. Godzik, Z. Gu and S. A. Lipton, *Science*, 2009, **324**, 102–105.
18 (*a*) K. Hensley and R. A. Floyd, *Arch. Biochem. Biophys.*, 2002, **397**, 377–383; (*b*) A. I. Bush, *Trends Neurosci.*, 2003, **26**, 207–214.
19 J. A. Duce and A. I. Bush, *Prog. Neurobiol.*, 2010, **92**, 1–18.
20 A. S. Pithadia and M. H. Lim, *Curr. Opin. Chem. Biol.*, 2012, **16**, 67–73.
21 T. D. Rae, P. J. Schmidt, R. A. Pufahl, V. C. Culotta and T. V. O'Halloran, *Science*, 1999, **284**, 805–808.

22 (*a*) K. J. Barnham and A. I. Bush, *Curr. Opin. Chem. Biol.*, 2008, **12**, 222–228; (*b*) S. C. Drew and K. J. Barnham, *Acc. Chem. Res.*, 2011, **44**, 1146–1155; (*c*) B. R. Roberts, T. M. Ryan, A. I. Bush, C. L. Masters and J. A. Duce, *J. Neurochem.*, 2012, **120**, 149–166; (*d*) L. E. Scott and C. Orvig, *Chem. Rev.*, 2009, **109**, 4885–4910.
23 M. A. Lovell, J. D. Robertson, W. J. Teesdale, J. L. Campbell and W. R. Markesbery, *J. Neurol. Sci.*, 1998, **158**, 47–52.
24 (*a*) L. M. Miller, Q. Wang, T. P. Telivala, R. J. Smith, A. Lanzirotti and J. Miklossy, *J. Struct. Biol.*, 2006, **155**, 30–37; (*b*) R. Squitti, *Front. Biosci., Landmark Ed.*, 2012, **17**, 451–472.
25 (*a*) A. I. Bush, W. H. Pettingell, G. Multhaup, M. d. Paradis, J.-P. Vonsattel, J. F. Gusella, K. Beyreuther, C. L. Masters and R. E. Tanzi, *Science*, 1994, **265**, 1464–1467; (*b*) D. P. Smith, G. D. Ciccotosto, D. J. Tew, M. T. Fodero-Tavoletti, T. Johanssen, C. L. Masters, K. J. Barnham and R. Cappai, *Biochemistry*, 2007, **46**, 2881–2891.
26 (*a*) X. Huang, C. S. Atwood, R. D. Moir, M. A. Hartshorn, R. E. Tanzi and A. I. Bush, *J. Biol. Inorg. Chem.*, 2004, **9**, 954–960; (*b*) D. J. Tew, S. P. Bottomley, D. P. Smith, G. D. Ciccotosto, J. Babon, M. G. Hinds, C. L. Masters, R. Cappai and K. J. Barnham, *Biophys. J.*, 2008, **94**, 2752–2766.
27 (*a*) X. Huang, C. S. Atwood, M. A. Hartshorn, G. Multhaup, L. E. Goldstein, R. C. Scarpa, M. P. Cuajungco, D. N. Gray, J. Lim, R. D. Moir, R. E. Tanzi and A. I. Bush, *Biochemistry*, 1999, **38**, 7609–7616; (*b*) X. Huang, M. P. Cuajungco, C. S. Atwood, M. A. Hartshorn, J. D. A. Tyndall, G. R. Hanson, K. C. Stokes, M. Leopold, G. Multhaup, L. E. Goldstein, R. C. Scarpa, A. J. Saunders, J. Lim, R. D. Moir, C. Glabe, E. F. Bowden, C. L. Masters, D. P. Fairlie, R. E. Tanzi and A. I. Bush, *J. Biol. Chem.*, 1999, **274**, 37111–37116.
28 (*a*) R. A. Cherny, J. T. Legg, C. A. McLean, D. P. Fairlie, X. Huang, C. S. Atwood, K. Beyreuther, R. E. Tanzi, C. L. Masters and A. I. Bush, *J. Biol. Chem.*, 1999, **274**, 23223–23228; (*b*) T. Storr, M. Merkel, G. X. Song-Zhao, L. E. Scott, D. E. Green, M. L. Bowen, K. H. Thompson, B. O. Patrick, H. J. Schugar and C. Orvig, *J. Am. Chem. Soc.*, 2007, **129**, 7453–7463.
29 D. R. Crapper McLachlan, A. J. Dalton, T. P. Kruck, M. Y. Bell, W. L. Smith, W. Kalow and D. F. Andrews, *Lancet*, 1991, **337**, 1304–1308.
30 (*a*) C. W. Ritchie, A. I. Bush, A. Mackinnon, S. Macfarlane, M. Mastwyk, L. MacGregor, L. Kiers, R. Cherny, Q.-X. Li, A. Tammer, D. Carrington, C. Mavros, I. Volitakis, M. Xilinas, D. Ames, S. Davis, K. Beyreuther, R. E. Tanzi and C. L. Masters, *Arch. Neurol. (Chicago)*, 2003, **60**, 1685–1691; (*b*) L. Lannfelt, K. Blennow, H. Zetterberg, S. Batsman, D. Ames, J. Harrison, C. L. Masters, S. Targum, A. I. Bush, R. Murdoch, J. Wilson and C. W. Ritchie, *Lancet Neurol.*, 2008, **7**, 779–786; (*c*) P. J. Crouch, M. S. Savva, L. W. Hung, P. S. Donnelly, A. I. Mot, S. J. Parker, M. A. Greenough, I. Volitakis, P. A. Adlard, R. A. Cherny, C. L. Masters, A. I. Bush, K. J. Barnham and A. R. White, *J. Neurochem.*, 2011, **119**, 220–230; (*d*) V. B. Kenche and K. J. Barnham, *Br. J. Pharmacol.*, 2011, **163**, 211–219; (*e*) L. Chiang, M. R. Jones, C. L. Ferreira and T. Storr, *Curr. Top. Med. Chem.*, 2012, **12**, 122–144; (*f*) D. Galimberti and E. Scarpini, *J. Neurol.*, 2012, **259**, 201–211.
31 (*a*) C. W. Ritchie, A. I. Bush, A. Mackinnon, S. Macfarlane, M. Mastwyk, L. MacGregor, L. Kiers, R. Cherny, Q.-X. Li, A. Tammer, D. Carrington, C. Mavros, I. Volitakis, M. Xilinas, D. Ames, S. Davis, K. Beyreuther, R. E. Tanzi and C. L. Masters, *Arch. Neurol. (Chicago)*, 2003, **60**, 1685–1691; (*b*) N. G. Faux, C. W. Ritchie, A. Gunn, A. Rembach, A. Tsatsanis, J. Bedo, J. Harrison, L. Lannfelt, K. Blennow, H. Zetterberg, M. Ingelsson, C. L. Masters, R. E. Tanzi, J. L. Cummings, C. M. Herd and A. I. Bush, *J. Alzheimers Dis.*, 2010, **20**, 509–516.
32 L. E. Scott, M. Telpoukhovskaia, C. Rodríguez-Rodríguez, M. Merkel, M. L. Bowen, B. D. G. Page, D. E. Green, T. Storr, F. Thomas, D. D. Allen, P. R. Lockman, B. O. Patrick, M. J. Adam and C. Orvig, *Chem. Sci.*, 2011, **2**, 642–648.
33 D. S. Folk and K. J. Franz, *J. Am. Chem. Soc.*, 2010, **132**, 4994–4995.
34 (*a*) L. K. Charkoudian, D. M. Pham and K. J. Franz, *J. Am. Chem. Soc.*, 2006, **128**, 12424–12425; (*b*) L. K. Charkoudian, D. M. Pham, A. M. Kwon, A. D. Vangeloff and K. J. Franz, *Dalton Trans.*, 2007, 5031–5042.
35 C. W. Tornøe, C. Christensen and M. Meldal, *J. Org. Chem.*, 2002, **67**, 3057–3064.
36 V. V. Rostovtsev, L. G. Green, V. V. Fokin and K. B. Sharpless, *Angew. Chem., Int. Ed.*, 2002, **41**, 2596–2599.
37 K. E. Djernes, O. Moshe, M. Mettry, D. D. Richards and R. J. Hooley, *Org. Lett.*, 2012, **14**, 788–791.
38 P. M. Guha, H. Phan, J. S. Kinyon, W. S. Brotherton, K. Sreenath, J. T. Simmons, Z. Wang, R. J. Clark, N. S. Dalal, M. Shatruk and L. Zhu, *Inorg. Chem.*, 2012, **51**, 3465–3477.
39 A. Boulay, A. Seridi, C. Zedde, S. Ladeira, C. Picard, L. Maron and E. Benoist, *Eur. J. Inorg. Chem.*, 2010, **32**, 5058–5062.
40 Z. P. Demko and K. B. Sharpless, *Org. Lett.*, 2001, **3**, 4091–4094.
41 V. Hong, S. I. Presolski, C. Ma and M. G. Finn, *Angew. Chem., Int. Ed.*, 2009, **48**, 9879–9883.
42 K. Asano and S. Matsubara, *Org. Lett.*, 2010, **12**, 4988–4991.
43 J. W. Lee, S. I. Jun and K. Kim, *Tetrahedron Lett.*, 2001, **42**, 2709–2711.
44 P. W. Betteridge, J. R. Carruthers, R. I. Cooper, K. Prout and D. J. Watkin, *J. Appl. Crystallogr.*, 2003, **36**, 1487.
45 L. Farrugia, *J. Appl. Crystallogr.*, 1997, **30**, 565.
46 T. D. Fenn, D. Ringe and G. A. Petsko, *J. Appl. Crystallogr.*, 2003, **36**, 944–947.
47 P. Gans, A. Sabatini and A. Vacca, *Ann. Chim.*, 1999, **89**, 45–49.
48 L. Alderighi, P. Gans, A. Ienco, D. Peters, A. Sabatini and A. Vacca, *Coord. Chem. Rev.*, 1999, **184**, 311–318.
49 B. Song, G. S. Kurokawa, S. Liu and C. Orvig, *Can. J. Chem.*, 2001, **79**, 1058–1067.
50 (*a*) S. S. Hindo, A. M. Mancino, J. J. Braymer, Y. Liu, S. Vivekanandan, A. Ramamoorthy and M. H. Lim, *J. Am. Chem. Soc.*, 2009, **131**, 16663–16665; (*b*) X. He, H. M. Park, S.-J. Hyung, A. S. DeToma, C. Kim, B. T. Ruotolo and M. H. Lim, *Dalton Trans.*, 2012, **41**, 6558–6566.
51 J.-S. Choi, J. J. Braymer, R. P. R. Nanga, A. Ramamoorthy and M. H. Lim, *Proc. Natl. Acad. Sci. U. S. A.*, 2010, **107**, 21990–21995.
52 J.-S. Choi, J. J. Braymer, S. K. Park, S. Mustafa, J. Chae and M. H. Lim, *Metallomics*, 2011, **3**, 284–291.
53 J. J. Braymer, J. S. Choi, A. S. DeToma, C. Wang, K. Nam, J. W. Kampf, A. Ramamoorthy and M. H. Lim, *Inorg. Chem.*, 2011, **50**, 10724–10734.
54 J. Jarvet, J. Danielsson, P. Damberg, M. Oleszczuk and A. Gräslund, *J. Biomol. NMR*, 2007, **39**, 63–72.
55 (*a*) S. Grzesiek, A. Bax, G. M. Clore, A. M. Gronenborn, J. S. Hu, J. Kaufman, I. Palmer, S. J. Stahl and P. T. Wingfield, *Nat. Struct. Biol.*, 1996, **3**, 340–345; (*b*) D. S. Garrett, Y.-J. Seok, A. Peterkofsky, G. M. Clore and A. M. Gronenborn, *Biochemistry*, 1997, **36**, 4393–4398; (*c*) M. P. Foster, D. S. Wuttke, K. R. Clemens, W. Jahnke, I. Radhakrishnan, L. Tennant, M. Reymond, J. Chung and P. E. Wright, *J. Biomol. NMR*, 1998, **12**, 51–71.
56 O. Trott and A. J. Olson, *J. Comput. Chem.*, 2009, **31**, 455–461.
57 G. M. Morris, R. Huey, W. Lindstrom, M. F. Sanner, R. K. Belew, D. S. Goodsell and A. J. Olson, *J. Comput. Chem.*, 2009, **30**, 2785–2791.
58 L. K. Wolf, *Chem. Eng. News*, 2009, **87**, 32.
59 M. Coles, W. Bicknell, A. A. Watson, D. P. Fairlie and D. J. Craik, *Biochemistry*, 1998, **37**, 11064–11077.
60 A. C. Stelzer, A. T. Frank, J. D. Kratz, M. D. Swanson, M. J. Gonzalez-Hernandez, J. Lee, I. Andricioaei, D. M. Markovitz and H. M. Al-Hashimi, *Nat. Chem. Biol.*, 2011, **7**, 553–559.
61 A. M. Mancino, S. S. Hindo, A. Kochi and M. H. Lim, *Inorg. Chem.*, 2009, **48**, 9596–9598.
62 C. W. Tornøe, C. Christensen and M. Meldal, *J. Org. Chem.*, 2002, **67**, 3057–3064.
63 A. Gero and J. J. Markham, *J. Org. Chem.*, 1951, **16**, 1835–1838.
64 (*a*) V. García, M. A. Garralda and L. Ibarlucea, *Transition Met. Chem. (Dordrecht, Neth.)*, 1985, **10**, 288–291; (*b*) R. C. Conrad and J. V. Rund, *Inorg. Chem.*, 1972, **11**, 129–134.
65 H. K. Hall, *J. Am. Chem. Soc.*, 1957, **79**, 5441–5444; D. A. Evans, http://evans.harvard.edu/pdf/evans_pka_table.pdf.
66 (*a*) H. K. Hall and R. B. Bates, *Tetrahedron Lett.*, 2012, **53**, 1830–1832; (*b*) A. G. Cook, L. R. Wesner and S. L. Folk, *J. Org. Chem.*, 1997, **62**, 7205–7209.
67 S.-R. Ji, Y. Wu and S.-f. Sui, *J. Biol. Chem.*, 2002, **277**, 6273–6279.

68 Given our unpublished ^{1}H–^{15}N TROSY-HSQC NMR data of HCl titrations against $A\beta_{1-40}$ monomer in SDS solution, which shows similar chemical shift perturbations (E11, H13, Q15, F20, and E22) in both direction and, to a lesser extent, magnitude.
69 S. F. Sousa, P. A. Fernandes and M. J. Ramos, *Proteins: Struct., Funct., Bioinf.*, 2006, **65**, 15–26; T. P. Lybrand, *Curr. Opin. Struct. Biol.*, 1995, **5**, 224–228.
70 W. L. Delano, 2002. The PyMOL Molecular Graphics System http://www.pymol.org, 2002.
71 (*a*) A. Rauk, *Dalton Trans.*, 2008, 1273–1282; (*b*) A. I. Bush, W. H. Pettingell, M. D. Paradis and R. E. Tanzi, *J. Biol. Chem.*, 1994, **269**, 12152–12158.
72 A. K. Sharma, S. T. Pavlova, J. Kim, D. Finkelstein, N. J. Hawco, N. P. Rath, J. Kim and L. M. Mirica, *J. Am. Chem. Soc.*, 2012, **134**, 6625–6636.
73 C. S. Atwood, R. D. Moir, X. Huang, R. C. Scarpa, N. M. Bacarra, D. M. Romano, M. A. Hartshorn, R. E. Tanzi and A. I. Bush, *J. Biol. Chem.*, 1998, **273**, 12817–12826.
74 A. E. Martell and R. J. Motekaitis, *Determination and Use of Stability Constants*, VCH, New York, 1988.
75 A. R. White, T. Du, K. M. Laughton, I. Volitakis, R. A. Sharples, M. E. Xilinas, D. E. Hoke, R. M. D. Holsinger, G. Evin, R. A. Cherny, A. F. Hill, K. J. Barnham, Q.-X. Li, A. I. Bush and C. L. Masters, *J. Biol. Chem.*, 2006, **281**, 17670–17680.
76 P. J. Crouch, L. W. Hung, P. A. Adlard, M. Cortes, V. Lal, G. Filiz, K. A. Perez, M. Nurjono, A. Caragounis, T. Du, K. Laughton, I. Volitakis, A. I. Bush, Q.-X. Li, C. L. Masters, R. Cappai, R. A. Cherny, P. S. Donnelly, A. R. White and K. J. Barnham, *Proc. Natl. Acad. Sci. U. S. A.*, 2009, **106**, 381–386.
77 (*a*) D. E. Ehrnhoefer, J. Bieschke, A. Boeddrich, M. Herbst, L. Masino, R. Lurz, S. Engemann, A. Pastore and E. E. Wanker, *Nat. Struct. Mol. Biol.*, 2008, **15**, 558–566; (*b*) J. Bieschke, J. Russ, R. P. Friedrich, D. E. Ehrnhoefer, H. Wobst, K. Neugebauer and E. E. Wanker, *Proc. Natl. Acad. Sci., U. S. A.*, 2010, **107**, 7710–7715; (*c*) A. R. A. Ladiwala, J. S. Dordick and P. M. Tessier, *J. Biol. Chem.*, 2011, **286**, 3209–3218.

